#### MINISTRY OF EDUCATION AND TRAINING

#### VIETNAM ACADEMY OF SCIENCE AND TECHNOLOGY

#### GRADUATE UNIVERSITY OF SCIENCE AND TECHNOLOGY



### Ha Minh Nguyet

STUDY ON THE SYNTHESIS OF TRANSITION METAL SULFIDE (Co, Cu, Mn) NANO MATERIALS FOR SUPERCAPACITOR ELECTRODE APPLICATIONS

SUMMARY OF DISSERTATION ON SCIENCES OF MATTER
Major: Inorganic Chemistry
Code: 9 44 01 13

The dissertation is completed at: Graduate University of Science and Technology, Vietnam Academy Science and Technology
Supervisors:  1. Supervisor 1: Assoc. Prof. Dr. Le Trong Lu  2. Supervisor 2: Prof. Dr. Le Anh Tuan
Referee 1:
Referee 2:
Referee 3:
The dissertation is examined by Examination Board of Graduate University of Science and Technology, Vietnam Academy of Science and Technology at(time, date)
The dissertation can be found at:  1. Graduate University of Science and Technology Library  2. National Library of Vietnam

#### INTRODUCTION

In recent years, a novel type of energy storage device, the supercapacitor, has garnered significant attention from both scientists and industry due to its superior properties. These properties include ultra-fast charge/discharge times (ranging from milliseconds to minutes), long cycle life (potentially exceeding 100,000 cycles), and high power density (in the range of kWkg<sup>-1</sup>). These characteristics position supercapacitors as that complement replace traditional components can or batteries/accumulators in applications demanding rapid charging, highpower delivery or consumption with continuous variation, or in applications requiring high charge/discharge stability.

However, compared to traditional batteries or capacitors, supercapacitors have not yet been widely adopted in practice due to their very low specific energy density (within the range of 5 – 80 Whkg<sup>-1</sup>, and commercial products typically 10 Whkg<sup>-1</sup>), which is significantly smaller than that of commonly used traditional batteries/accumulators (approx. 170 Whkg<sup>-1</sup>). This low energy density results in supercapacitors having a much larger size compared to batteries/capacitors for the same amount of stored energy. Developing supercapacitors with a higher energy density to approach that of current rechargeable batteries, while retaining their unique superior characteristics, is currently a major global research trend.

The most common way to increase the energy density of supercapacitors is to enhance the specific capacitance of the electrode material. Based on the energy storage mechanism, the specific capacitance of supercapacitor electrode materials is being developed along two main directions: (1) Synthesizing materials with a large specific surface area to enhance the electrical double-layer capacitance (EDLC) effect; (2)

Synthesizing electrode materials capable of participating in reversible redox reactions to improve the pseudocapacitance effect.

The recent research trend is the development of hybrid materials that simultaneously combine both of these effects. These materials need to concurrently meet two requirements: the materials must have a nanostructure and their elemental composition must include multivalent elements. Nanostructured materials offer a larger surface area and a shorter diffusion path for charge carriers, thereby accelerating the Faradaic electron-transfer reactions. Based on these requirements, transition metal compounds with various oxidation states that can be flexibly and reversibly interconverted, and diverse, easily controllable morphologies, have attracted the attention of numerous research groups both domestically and internationally. Among transition metal compounds, sulfides exhibit superior electrochemical properties due to their better electrical conductivity and mechanical stability.

Based on the above analysis, the thesis, "Study on the synthesis of transition metal sulfide (Co, Cu, Mn) nano materials for supercapacitor electrode applications" was conducted with the following objectives and content:

## **Objectives of the thesis**

- Fabricate and characterize the transition metal sulfide (Co, Cu, Mn) nano materials.
- Evaluate the electrochemical properties of the fabricated materials when used as supercapacitor electrodes.

## **Research content**

- Synthesis and characterization of transition metal sulfide nano materials
- Fabrication and electrochemical performance of hybrid supercapacitor electrodes developed from the synthesized materials.

- Fabrication and electrochemical performance of supercapacitor prototypes using the prepared hybrid electrodes.

#### **CHAPTER 1. OVERVIEW**

## 1.1. Energy storage and conversion devices

Based on the energy storage mechanism, supercapacitors are primarily divided into two main types: EDLCs and Pseudocapacitors. Generally, EDLCs possess high power density, whereas electrochemical pseudocapacitors exhibit higher energy density. Therefore, the current research trend is to combine both of these energy storage mechanisms to create **hybrid supercapacitors**.

#### 1.2. Electrode materials for supercapacitors

Carbon-based materials are commonly used as electrodes for EDLCs. Transition metal compounds and conductive polymers are typically employed as electrodes for electrochemical pseudocapacitors. Hybrid supercapacitors utilize a combination of carbon-based materials with conductive polymers or metal oxides as electrodes.

#### 1.3. Transition metal sulfide-based electrode materials

Transition metals possess multiple valence states. Consequently, transition metal sulfides exhibit diversity in crystal structure, morphology, shape, size, and elemental composition. For this reason, they have become a potential research subject in many fields, including their application as electrode materials for supercapacitors.

#### **CHAPTER 2. MATERIALS AND METHODS**

## 2.1. Reagents and chemicals

## 2.2. Experimental procedure

## 2.2.1. Fabrication of CoS-based electrodes

CoS was synthesized using two different procedures: a one-step hydrothermal method performed at various reaction times and an anion

exchange reaction utilizing two different sulfur sources. The CoS/CNT electrodes were fabricated by direct 3D printing onto a graphite substrate.

#### 2.2.2. Fabrication of CuCo<sub>2</sub>S<sub>4</sub>-based electrodes

rGO (reduced Graphene Oxide) was fabricated by reducing GO using the modified Hummer's method. The CuCo<sub>2</sub>S<sub>4</sub> composite material was synthesized via the hydrothermal method from rGO and inorganic salts. The CuCo<sub>2</sub>S<sub>4</sub>/CNTelectrodes were fabricated by direct 3D printing onto a graphite substrate combined with freeze gelation.

### 2.2.3. Fabrication of MnCo<sub>2</sub>S<sub>4</sub>-based electrodes

Fabrication of MnCo<sub>2</sub>S<sub>4</sub>-NS Electrodes

 $MnCo_2S_4$  nanosheet ( $MnCo_2S_4$ -NS) material was synthesized using the spray pyrolysis method and then functionalized with  $NOBF_4$  to enhance its dispersibility in polar solvents. The printing ink consisted of the  $NOBF_4$ -functionalized  $MnCo_2S_4$ -NS dispersed in DMF solvent and was printed onto a graphite substrate.

## Fabrication of MnCo<sub>2</sub>S<sub>4</sub>/rGO electrodes

 $MnCo_2S_4$  nanosphere ( $MnCo_2S_4$  NPs) material was synthesized using the spray pyrolysis method and then functionalized with NOBF<sub>4</sub> to enhance its dispersibility in polar solvents. The printing ink for electrode fabrication consisted of  $MnCo_2S_4$ -NPs,  $MnCo_2S_4$ /rGO and PVP dispersed in DMF and was printed onto a graphite substrate.

### 2.2.4. Electrochemical performance of supercapacitor prototype

Supercapacitor prototypes were fabricated to evaluate the practical application potential of the  $MnCo_2S_4$ -based electrode materials.

## 2.3. Characterization Techniques

The characterization techniques included: Electron Microscopy, Energy-Dispersive X-ray Spectroscopy, X-ray Diffraction, X-ray Photoelectron Spectroscopy, Viscosity Measurement, Thermogravimetric Analysis.

#### 2.4. Electrochemical Methods

The electrochemical methods included: Cyclic Voltammetry, Galvanostatic Charge-Discharge, Electrochemical Impedance Spectroscopy.

#### **CHAPTER 3. RESULTS AND DISCUSSION**

#### 3.1. Synthesis and Characterization of CoS-based Electrode Materials

### 3.1.1. CoS material synthesized by hydrothermal Method

#### 3.1.1.1. Characterization of CoS material

SEM images show that the development of the CoS crystal morphology is strongly dependent on the reaction time.

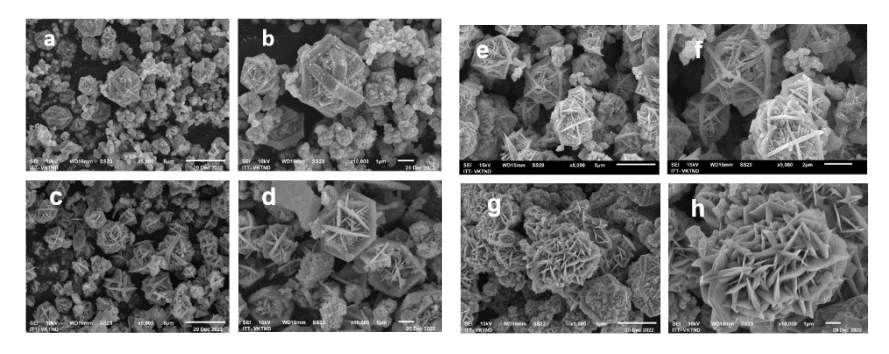


Fig 3.1. SEM images of CoS material synthesized at different reaction times: 3 hours (a, b), 6 hours (c, d), 9 hours (e, f), and 12 hours (g, h)

The XRD patterns of CoS-3 and CoS-6 both show characteristic peaks corresponding to the crystal structure of the mineral Jaipurite – hexagonal CoS (JCPDS#65 – 3418), while the crystallinity of CoS-6 is better than that of CoS-3.

## 3.1.1.2. Electrochemical performance of CoS/CNT electrodes

The CV curves of all four CoS/CNT electrodes are distorted compared to a rectangular shape, with redox peaks corresponding to the

reversible processes of the Co<sup>2+</sup>/Co<sup>3+</sup> and Co<sup>3+</sup>/Co<sup>4+</sup> couples in 6M KOH solution, with the specific capacitance of CoS-6/CNT being the largest.

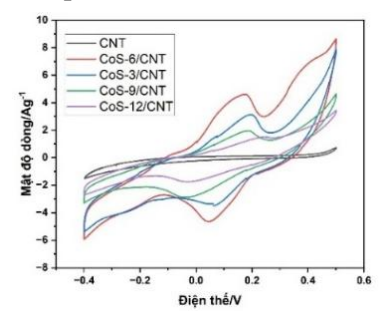


Fig 3.5. CV curves in 6M KOH solution of CoS/CNT electrodes at a scan rate of 5 mVs<sup>-1</sup>

Results from the CV analysis using the Dunn method show that the CoS/CNT electrodes are hybrid electrodes.

The CV results show that CoS-6/CNT exhibits the best electrochemical performance; therefore, this electrode was selected for the charge-discharge stability test. The specific capacitance of the CoS-6/CNT electrode at 2.5 Ag<sup>-1</sup> is 380.5 Fg<sup>-1</sup>. After 3000 charge-discharge cycles at 50 Ag<sup>-1</sup>, the specific capacitance of the electrode showed a rapid initial decline but then stabilized and only dropped by 7.3%.

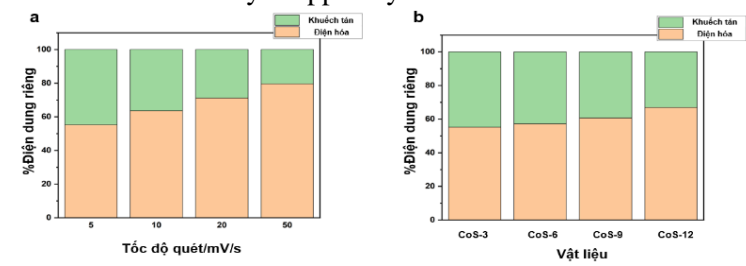


Fig 3.8. Comparison of the contributions of the diffusion process and the capacitive process of CoS/CNT electrodes: (a) CoS-6/CNT at various scan rates, (b) CoS/CNT electrodes at a scan rate of 5 mVs<sup>-1</sup>

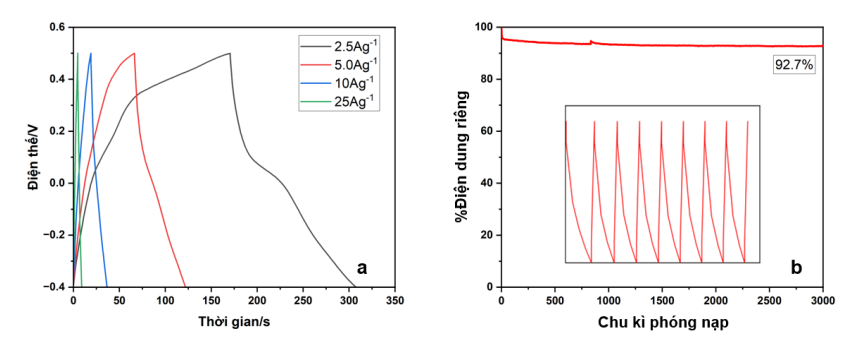


Fig 3.9. GCD curves of the CoS-6/CNT electrode at various current densities and charge-discharge stability of the material after 3000 cycles

Results from the investigation show that the Coulombic efficiency of the CoS-6/CNT electrode reached its highest value of 87.8% in the initial cycles, then quickly dropped to 85% and subsequently stabilized.

## 3.1.2. CoS Material Synthesized by Anion Exchange Method

### 3.1.2.1. Characterization of CoS Material

After the anion exchange reaction, the characteristic peak of S element is clearly visible in both CoS-SS and CoS-TU materials. OXRD pattern shows that the cobalt oxide framework has characteristic peaks corresponding to the Co<sub>3</sub>O<sub>4</sub> material. The patterns of CoS-SS and CoS-TU both show characteristic peaks of the CoS phase. The Co 2p XPS spectrum is divided into 4 peaks, in which the Co 2p3/2 and Co 2p1/2 peaks have binding energies of 780.9 and 796.7 eV, respectively, confirming the existence of Co<sup>2+</sup>. In the S 2p XPS spectrum, the two peaks at S1 162.5 and S2 164.0 eV correspond to the S<sup>2-</sup> ion and sulfur atoms in a covalent bond, respectively.

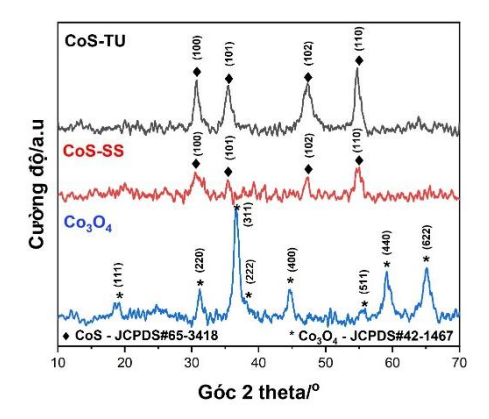


Fig 3.14. XRD patterns of Co<sub>3</sub>O<sub>4</sub>, CoS-SS và CoS-TU

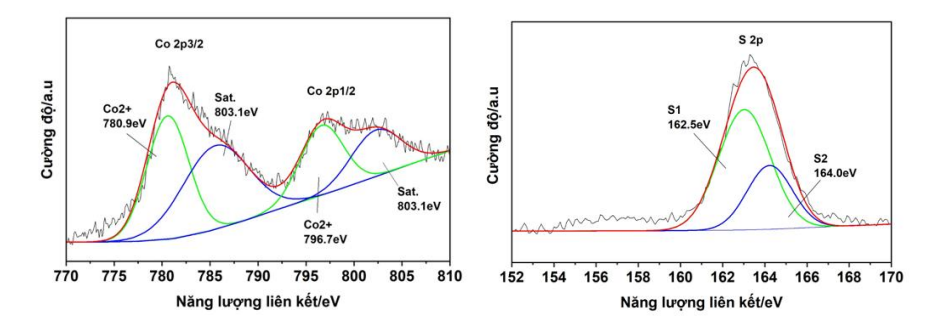


Fig 3.15. XPS spectra of Co 2p and S 2p

## 3.1.2.2. Electrochemical performance of CoS/CNT electrodes

The area of the CV curve of the CNT electrode is very small, negligible compared to the area of the CV curves of the other electrodes. The specific capacitance values of the  $Co_3O_4/CNT$ , CoS-SS/CNT, and CoS-TU/CNT electrodes are 670, 1137, and 1573  $Fg^{-1}$  respectively. Thus, the

anion exchange has helped increase the electrochemical performance of the corresponding oxide.

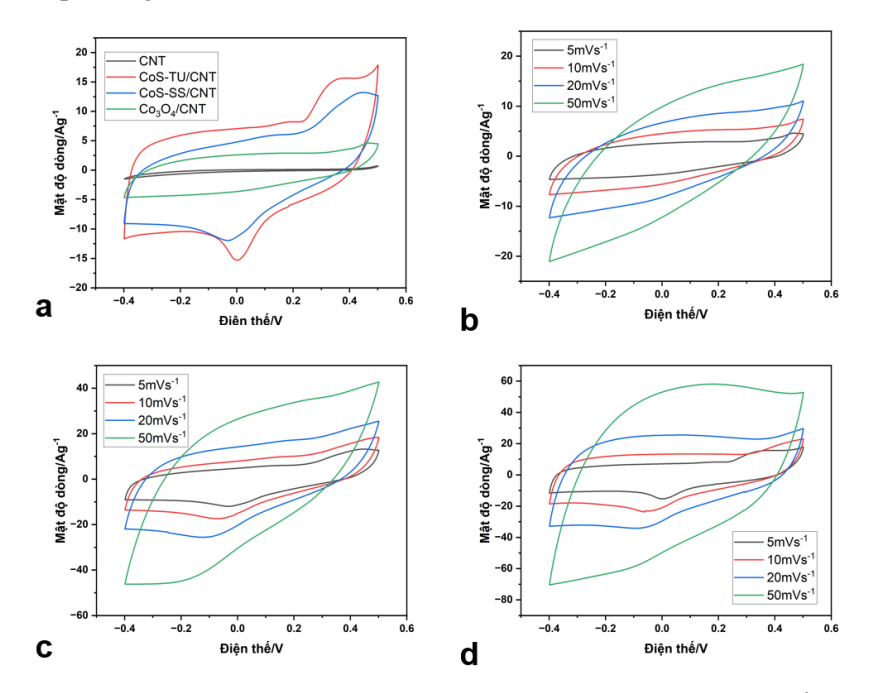


Fig 3.16. CV curves in KOH 6M solution of (a) electrodes at 5 mVs<sup>-1</sup>, and electrodes at different scan rates:  $Co_3O_4/CNT$ , (c) CoS-SS/CNT và (d) CoS-TU/CNT

In general, all materials store energy via both mechanisms. The electrochemical process predominantly controls the behavior of the Co<sub>3</sub>O<sub>4</sub>/CNT electrode, with a very low contribution from the diffusion process. Following the anion exchange reaction, although the electrochemical process remains dominant, the contribution of the diffusion process in both CoS-SS/CNT, and CoS-TU/CNT electrodes increased significantly compared to the oxide. The efficiency of energy storage through

both mechanisms for the CoS synthesized by the anion exchange method is higher than for the CoS synthesized by the one-step hydrothermal method.

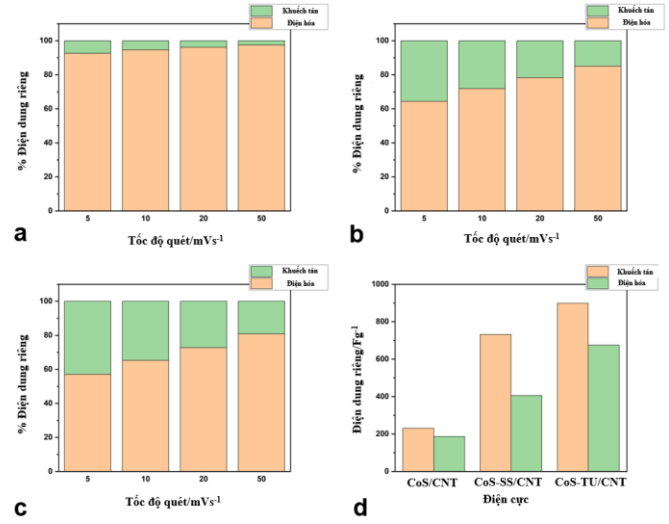


Fig 3.18. Contribution of the two energy storage processes of the electrodes: (a)  $Co_3O_4/CNT$ , (b) CoS-SS/CNT), (c) CoS-TU/CNT and (d) comparison of the specific capacitance of each process for the electrodes

After 5000 charge-discharge cycles, the specific capacitance of the  $\text{Co}_3\text{O}_4/\text{CNT}$  electrode dropped sharply, retaining only 61% of its initial value. Meanwhile, the specific capacitance of CoS-SS/CNT and CoS-TU/CNT did not decrease significantly after numerous electrochemical cycles, both retaining over 96% of their initial value. The impedance spectra of the electrodes were performed in the frequency range of 100 kHz – 10 mHz. The  $R_s$  of the electrodes  $\text{Co}_3\text{O}_4/\text{CNT}$ , CoS-SS/CNT and CoS-TU/CNT are 1.32, 0.99, and 0.78  $\Omega$ , respectively. The Coulombic efficiency of CoS-SS/CNT and CoS-TU/CNT was initially approximately equal (90.4% and 90.1%), but in the first 100 charge-discharge cycles, CoS-SS/CNT decreased faster than CoS-TU/CNT.

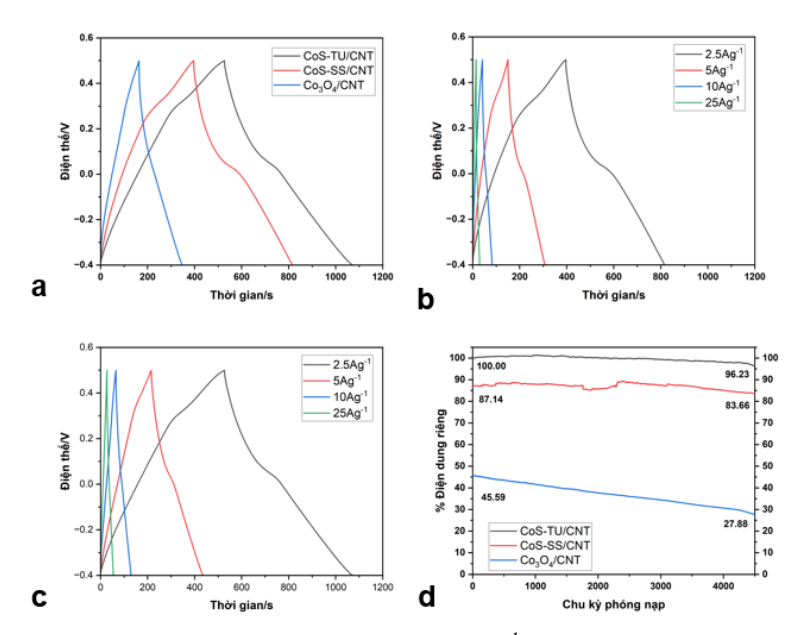


Fig 3.19. GCD curves of electrodes at 2.5 Ag<sup>-1</sup> (a), electrodes at different current densities: (b) CoS-SS.CNT, (c) CoS-TU/CNT, and (d) comparision of charge-discharge stability

# 3.2. Synthesis and characterization of $CuCo_2S_4-$ based electrode

### 3.2.1. Fabrication of CuCo<sub>2</sub>S<sub>4</sub>/rGO electrode

TEM and HR-TEM images show that  $CuCo_2S_4$  consists of spherical nanoparticles with an average size of 5-10 nm anchored onto the surface of rGO. The XRD pattern of the composite material exhibits diffraction peaks of crystalline  $CuCo_2S_4$ . The  $CuCo_2S_4$ /rGO electrode has a porous surface with various pore sizes. Voids were formed due to the intercalation and subsequent sublimation of phenol. These pores increase the contact area between the material and the electrolyte, thereby improving ion exchange capability and accelerating electron-transfer reactions.

EDS analysis confirmed the presence of Cu, Co, and S elements on the electrode. The atomic ratio of these elements is 1:2:4, corresponding to the spinel structure of  $CuCo_2S_4$ . The EDX mapping shows that the elements are uniformly distributed throughout the material sample.

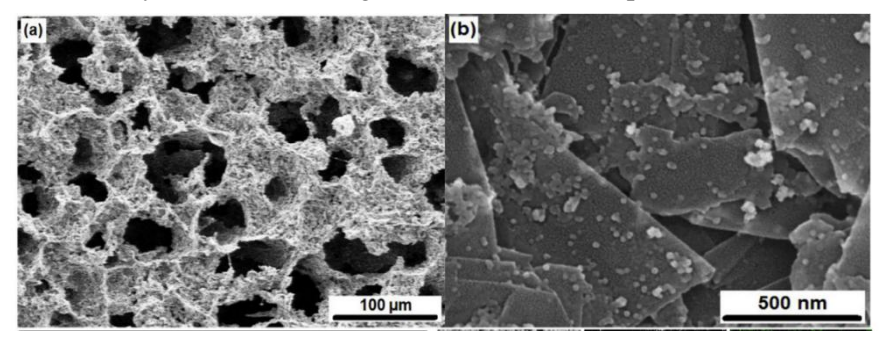


Fig 3.24. SEM images of CuCo<sub>2</sub>S<sub>4</sub>/rGO electrode

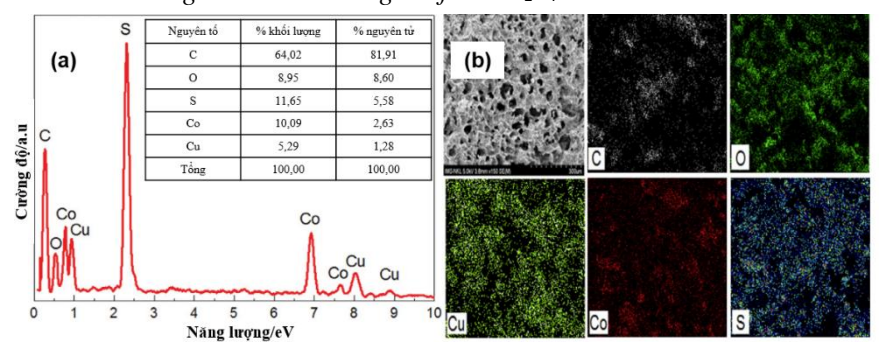


Fig 3.25. EDX spectrum (a) and EDX mapping (b) of CuCo<sub>2</sub>S<sub>4</sub>/rGO electrode

### 3.2.2. Capacitive performance of CuCo<sub>2</sub>S<sub>4</sub>/rGO electrode

The CV curve of the  $CuCo_2S_4/rGO$  electrode clearly shows reversible redox peaks. These redox peaks correspond to the conversion processes of the  $Cu^{2+}/Cu^{1+}$  and  $Co^{4+}/Co^{3+}$  couples in an alkaline environment. The overall shape of the CV curve is close to a rectangular shape, indicating the electrical double-layer capacitance effect. That is, the  $CuCo_2S_4/rGO$ 

composite material is a hybrid material capable of storing energy via both mechanisms. Furthermore, the shape of the CV curve did not change significantly when the scan rate was increased by 10 times (from 5 to 50 mVs<sup>-1</sup>). This indicates that the composite material operates stably even at high scan rates. The specific capacitance of the material calculated from the area of the CV curve is 1123 Fg<sup>-1</sup> at a scan rate of 5 mVs<sup>-1</sup>. Even at a very fast scan rate of 50 mVs<sup>-1</sup>, the contribution of the diffusion process to the behavior of the CuCo<sub>2</sub>S<sub>4</sub>/rGO electrode still amounts to nearly 30%, demonstrating that the porous nanostructure of the CuCo<sub>2</sub>S<sub>4</sub>/rGO electrode has helped shorten the diffusion path of ions in the electrolyte into the electrode material.

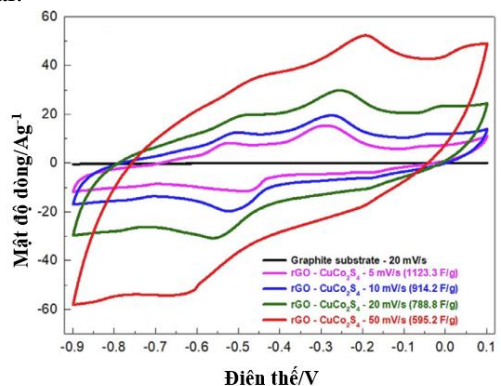


Fig 3.26. CV curves at different scan rate of  $CuCo_2S_4/rGO$  electrode When the current density increased by 5 times  $(2-10~Ag^{-1})$ , the specific capacitance of  $CuCo_2S_4/rGO$  in this study only decreased by 1.7 times when the current density increased by 8 times  $(5-40~Ag^{-1})$ . These values indicate the fast rate of the redox reactions on the surface of the  $CuCo_2S_4/rGO$  electrode.

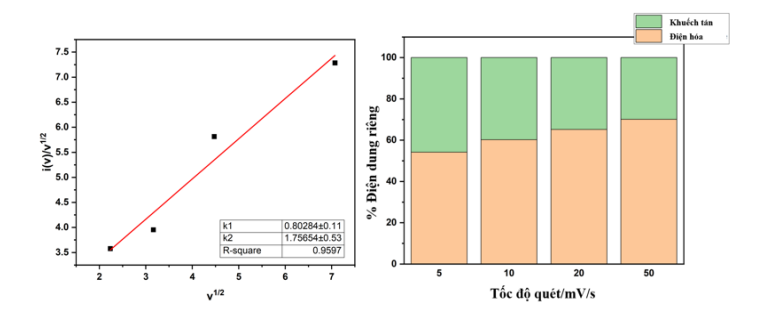


Fig 3.27. Plot of  $(v)/v^{1/2}$  vs  $v^{1/2}$  and the contribution of the two energy storage processes of the  $CuCo_2S_4/rGO$  electrode

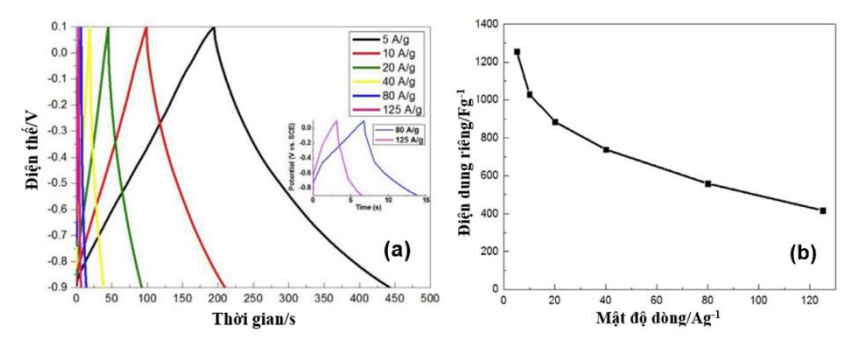


Fig 3.28. GCD curves (a) and specific capacity at different current densities (b) of the CuCo<sub>2</sub>S<sub>4</sub>/rGO electrode

The specific capacity of CuCo<sub>2</sub>S<sub>4</sub>/rGO decreased 9% after 20000 cycles. The Coulombic efficiency was 99.8% at initial cycles and reduced insignificantly (retained 99.3%) after thousands of cycles.

## 3.3. Synthesis and characterization of MnCo<sub>2</sub>S<sub>4</sub>-based electrodes

### 3.3.1. $MnCo_2S_4$ –NS

## 3.3.1.1. Morphology analysis

The material is nanostructured with particles with thickness and length of 10 nm and 80-100 nm, respectively. The BET surface area is 127  $m^2g^{-1}$ .

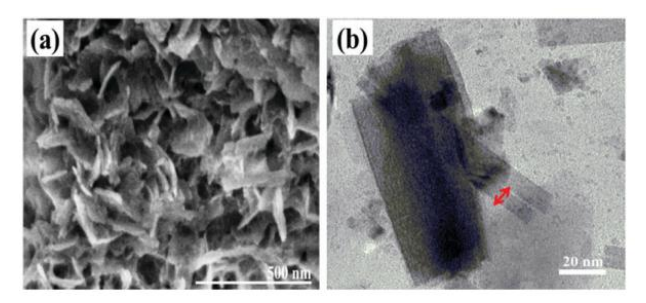


Fig 3.32. (a) SEM and (b) TEM images of MnCo<sub>2</sub>S<sub>4</sub> –NS

The XRD analysis results show peaks at  $31.7^{\circ}$ ,  $38.2^{\circ}$ ,  $50.3^{\circ}$  and  $55.3^{\circ}$  corresponding to the (222), (400), (511), and (440) planes of the spinel crystal MnCo<sub>2</sub>S<sub>4</sub> –NS. The atomic percentage of Mn, Co, and S elements are 9.65, 20.12, and 46.34, respectively, which corresponds to the ratio in the MnCo<sub>2</sub>S<sub>4</sub> –NS formula. The distribution of the main elements MnCo<sub>2</sub>S<sub>4</sub> –NS is quite uniform, as shown in the elemental map.

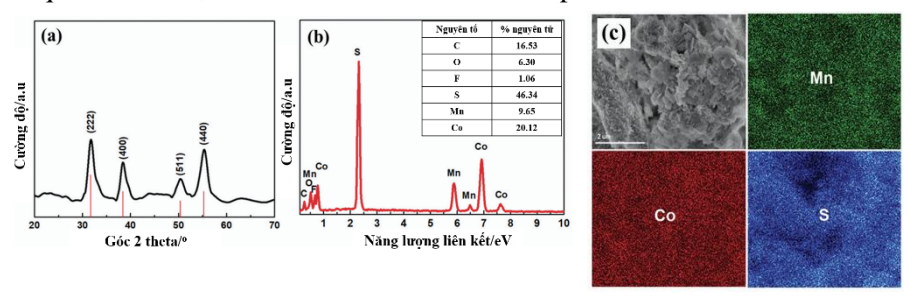


Fig 3.34. (a) XRD pattern, (b) EDX spectrum and (c) EDX mapping of MnCo<sub>2</sub>S<sub>4</sub> -NS

After 5000 charge-discharge cycles, the  $MnCo_2S_4$  –NS material still retains its porous nanostructure, although the surface is rougher. The presence of the Mn, Co, and S peaks indicates that the  $MnCo_2S_4$  –NS material

remains bonded to the graphite substrate after numerous charge-discharge cycles without the use of a binder.

## 3.3.1.2. Capacitive performance

The CV curve of the  $MnCo_2S_4$  –NS electrode shows a pair of reversible redox peaks corresponding to the  $Co^{2+}/Co^{3+}$  and  $Mn^{2+}/Mn^{3+}$  couples in a KOH environment. The diffusion process predominantly controls the behavior of the  $MnCo_2S_4$  –NS electrode, meaning that the nanosheet structure of the material facilitated better ion diffusion, thereby improving the electrochemical performance of the electrode.

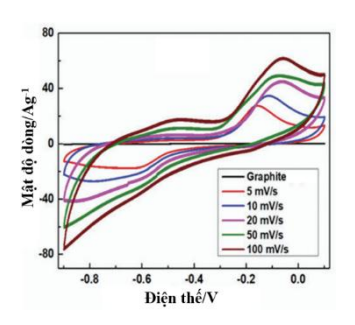


Fig 3.38. CV curves of MnCo<sub>2</sub>S<sub>4</sub> – NS at different scan rate

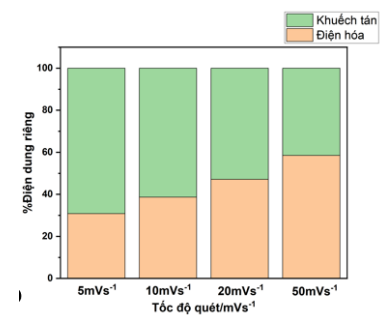


Fig 3.39. The contribution of the two energy storage processes of MnCo<sub>2</sub>S<sub>4</sub> –NS electrode

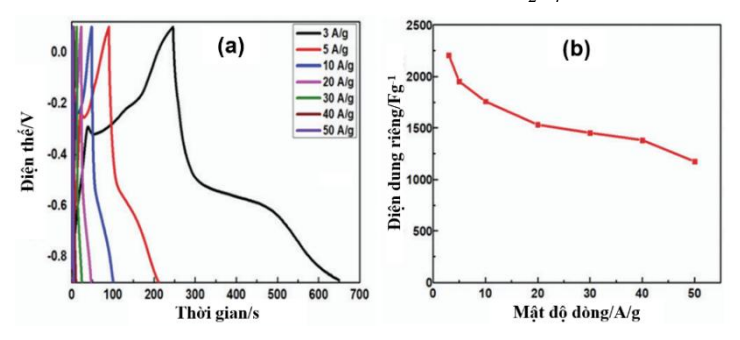


Fig 3.40. GCD curves (a) and specific capacity of MnCo<sub>2</sub>S<sub>4</sub> –NS electrode at different current densities

The specific capacitance of the  $MnCo_2S_4$  –NS electrode at various current densities decreased from 2203.6 to 1173.4 Fg<sup>-1</sup> when the current density increased from 3 to 50 Ag<sup>-1</sup>. After 5000 cycles, the specific capacitance of the  $MnCo_2S_4$  –NS electrode decreased from 1173.4 Fg<sup>-1</sup> to 1092.6 Fg<sup>-1</sup>, meaning the remaining specific capacitance value is 93% of the initial value.

The Nyquist plots of the  $MnCo_2S_4$  –NS electrode before and after 5000 charge-discharge cycles have similar shapes. The solution resistance  $R_s$  in both impedance spectra is low, at  $0.62\Omega$  for the initial  $MnCo_2S_4$  –NS electrode and  $0.65\Omega$  for the electrode after 5000 charge-discharge cycles, meaning that the  $MnCo_2S_4$  –NS and the graphite substrate remained tightly bound throughout the testing.

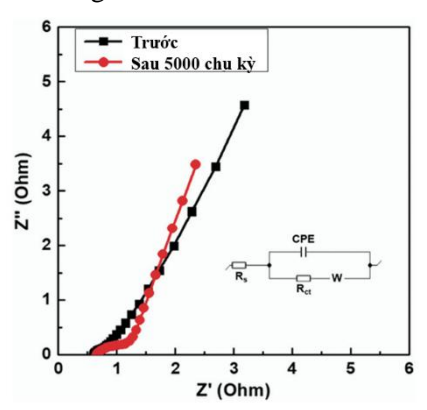


Fig 3.43. Nyquist plot before and after 5000 cycles and equivalent circuit of MnCo<sub>2</sub>S<sub>4</sub> –NS electrode

### 3.3.1.3. Electrochemical performance of supercapacitor prototype

The CV curve of the supercapacitor has an asymmetric shape with redox peak pairs in the range of 1.1 - 1.2 and 1.5 - 1.7 V. The operating voltage window of 1.7 V is a relatively wide potential range for a supercapacitor, contributing to the high energy density of the device. The

specific capacitance calculated based on the total mass of the negative and positive electrodes of the supercapacitor are 239, 215, 186, 165, 136, 107 and 76 Fg<sup>-1</sup> at current densities of 2, 3, 4, 6, 8 and 10 Ag<sup>-1</sup> respectively. The ability to operate at a high current density up to 10 Ag<sup>-1</sup> shows that the supercapacitor has good rate capability and is suitable for high-power applications. The Ragone plot of the symmetric MnCo<sub>2</sub>S<sub>4</sub> –NS// MnCo<sub>2</sub>S<sub>4</sub> – NS supercapacitor shows that when the energy density of the device reaches its maximum value of 96 Whkg<sup>-1</sup>, the power density is 1857 Whkg<sup>-1</sup>, and when the energy density decreases to 30 Whkg<sup>-1</sup>, the corresponding power density is 11660 Whkg<sup>-1</sup>.

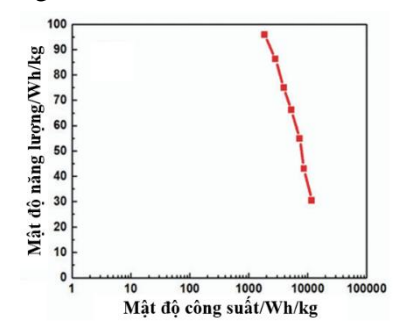


Fig 3.46. Ragone plot of MnCo<sub>2</sub>S<sub>4</sub>–NS supercapacitor

## 3.3.2. MnCo<sub>2</sub>S<sub>4</sub>/rGO

### 3.3.2.1. Morphology analysis

TEM images of the  $MnCo_2S_4$ -NPs nanoparticles show that the material has a spherical shape with an average size of about 10 nm and high uniformity. The rGO sheets are very thin, like silk materials folded together. After sonication, the  $MnCo_2S_4$ -NPs were anchored onto the rGO material with a relatively high density. The combination of rGO and  $MnCo_2S_4$ -NPs helped increase the BET surface area of the composite material to 836  $m^2g^{-1}$ 

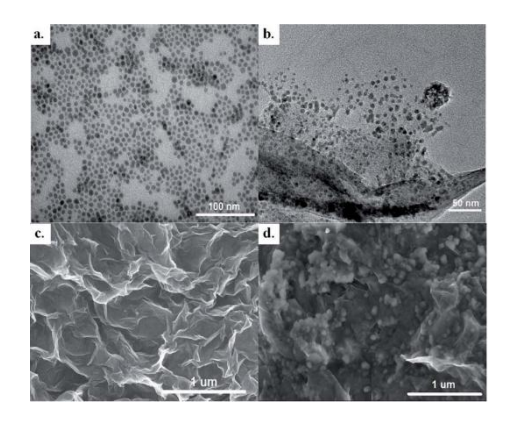


Fig 3.48. TEM images of (a) MnCo<sub>2</sub>S<sub>4</sub>-NPs and (b) MnCo<sub>2</sub>S<sub>4</sub>/rGO, SEM images of (c) rGO and (d) MnCo<sub>2</sub>S<sub>4</sub>/rGO

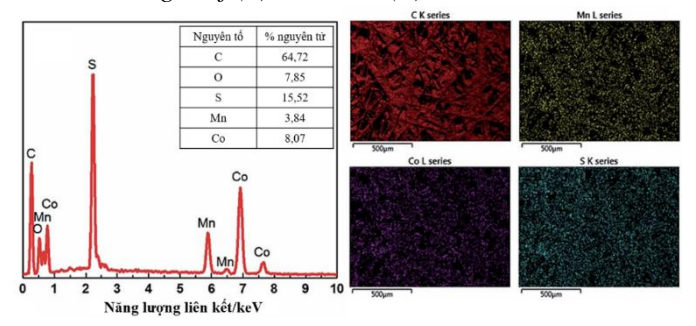


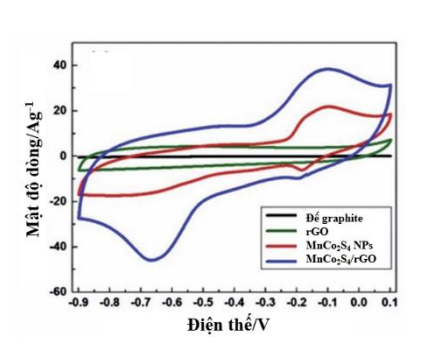
Fig 3.51. Elemental composition and EDX mapping of MnCo<sub>2</sub>S<sub>4</sub>/rGO

The XRD pattern of MnCo<sub>2</sub>S<sub>4</sub>-NPs shows the characteristic peaks of this material. The XRD pattern of MnCo<sub>2</sub>S<sub>4</sub>-NPs/rGO shows the characteristic peaks of the individual MnCo<sub>2</sub>S<sub>4</sub>-NPs and rGO materials, however, the signal intensity is lower compared to these two initial material samples. EDS analysis and the mapping of MnCo<sub>2</sub>S<sub>4</sub>-NPs/rGO show the presence of the elements Co, Mn, S, C, and O, in which the atomic ratio of Co/Mn is 8.07/3.84, closest to the MnCo<sub>2</sub>S<sub>4</sub> formula. The elements are uniformly distributed over the entire electrode surface, meaning that the

MnCo<sub>2</sub>S<sub>4</sub>-NPs were uniformly distributed on the rGO layers and this composite material was well dispersed in the DMF solvent.

### 3.3.2.2. Electrochemical performance

The CV curve of MnCo<sub>2</sub>S<sub>4</sub>-NPs shows redox peaks demonstrating reversible charge transfer reactions of the Co<sup>2+</sup>/Co<sup>3+</sup>/Co<sup>4+</sup> and Mn<sup>2+</sup>/Mn<sup>3+</sup> ion couples. Meanwhile, the CV curve of MnCo<sub>2</sub>S<sub>4</sub>-NPs/rGO has both a rectangular shape and distinct redox peaks. The cathodic peak of the MnCo<sub>2</sub>S<sub>4</sub>-NPs/rGO composite material is even higher than that of the initial MnCo<sub>2</sub>S<sub>4</sub>-NPs material. At the same scan rate of 5 mVs<sup>-1</sup>, the specific capacitance of the rGO, MnCo<sub>2</sub>S<sub>4</sub>-NPs, and MnCo<sub>2</sub>S<sub>4</sub>-NPs/rGO materials are 409, 2097, and 3339 Fg<sup>-1</sup> respectively. This shows that the combination of MnCo<sub>2</sub>S<sub>4</sub>-NPs and rGO not only inherits the advantages of the individual materials but also benefits from mutual enhancement.



. Fig 3.52. CV curves of MnCo<sub>2</sub>S<sub>4</sub>
–NPs-based electrodes at 5mVs<sup>-1</sup>

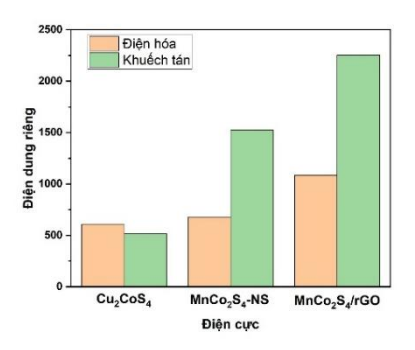


Fig 3.55. Comparison of the CuCo<sub>2</sub>S<sub>4</sub> and MnCo<sub>2</sub>S<sub>4</sub> based electrodes at 5mVs<sup>-1</sup>

MnCo<sub>2</sub>S<sub>4</sub>-NPs/rGO is a hybrid electrode, where the diffusion process is more dominant than the purely capacitive process at the electrode surface. The incorporation of rGO into the MnCo<sub>2</sub>S<sub>4</sub>-NPs material significantly increased the contribution of both energy storage mechanisms,

suggesting that rGO created a conductive network and an ideal nanostructure, optimizing ion and electron transport. The maximum specific capacitance of MnCo<sub>2</sub>S<sub>4</sub>-NPs/rGO is 3812.5 Fg<sup>-1</sup> at a current density of 2 Ag<sup>-1</sup>. After 22000 cycles, the specific capacitance of the MnCo<sub>2</sub>S<sub>4</sub>-NPs/rGO electrode reached 92.2% of its initial specific capacitance. After 22000 cycles, the Coulombic efficiency of MnCo<sub>2</sub>S<sub>4</sub>-NPs/rGO still reached 93.1%. The decrease in Coulombic efficiency and the initial values exceeding 100% are attributed to the surface active agents of MnCo<sub>2</sub>S<sub>4</sub>-NPs/rGO. The impedance and charge transfer resistance of the MnCo<sub>2</sub>S<sub>4</sub>-NPs/rGO electrode are quite low,  $R_s = 1.087\Omega$  and  $Rct = 0.025\Omega$ . After 22000 cycles, these values increased but remained low,  $R_s = 1.172\Omega$  and  $R_{ct} = 0.078\Omega$ , once again confirming the efficient electrochemical performance of the MnCo<sub>2</sub>S<sub>4</sub>-NPs/rGO electrode.

### 3.3.2.3. Electrochemical performance of supercapacitor prototype

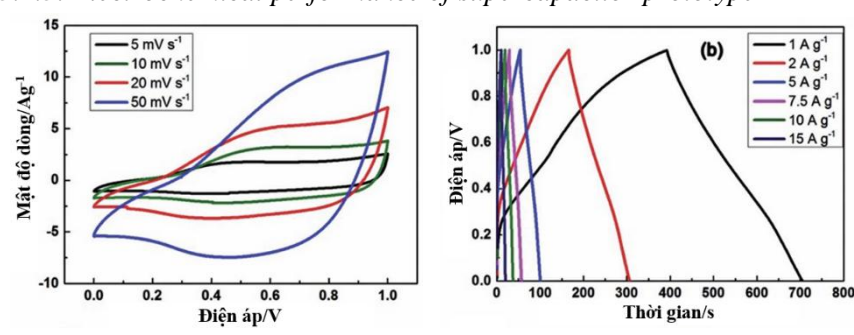


Fig 3.60. CV curves of MnCo<sub>2</sub>S<sub>4</sub>/rGO supercapacitor

Fig 3.61. GCD curves of MnCo<sub>2</sub>S<sub>4</sub>/rGO supercapacitor

The specific capacitance of the supercapacitor are 316.2, 288.7, 244.7, 222.6, 200.0 and 157.7 Fg<sup>-1</sup> at current densities of 1, 2, 5, 7.5, 10 and 15 Ag<sup>-1</sup> respectively. The maximum energy density reached 43.91 Whkg<sup>-1</sup>, corresponding to a power density of 505 Whkg<sup>-1</sup>. When the energy density dropped to 21.9 Whkg<sup>-1</sup>, the maximum power density reached 8762 Whkg<sup>-1</sup>.

#### CONCLUSION AND RECOMMENDATION

#### **CONCLUSION**

The dissertation successfully synthesized five transition metal sulfide nanomaterial systems. All electrodes exhibited an energy storage mechanism combining ion diffusion and Faradaic electrochemical reactions.

The CoS material synthesized by the one-step hydrothermal method had a layered nanosheet structure, high crystallinity, and uniform morphology. The CoS-3/CNT electrode achieved a maximum specific capacitance of 380.5 Fg<sup>-1</sup> at 2.5 Ag<sup>-1</sup>. The anion exchange method significantly improved the electrochemical activity compared to hydrothermally synthesized CoS. The CoS-SS/CNT and CoS-TU/CNT electrodes achieved specific capacitances of 1236 and 1502 Fg<sup>-1</sup> at 2.5 Ag<sup>-1</sup>, maintaining over 96% capacity after 5000 cycles.

The sublimation of phenol during the synthesis created a 3D nanoporous structure for the  $CuCo_2S_4/rGO$  electrode, increasing the contact area between the electrolyte and the active surface, thereby significantly improving the electrochemical performance. The material achieved a specific capacitance of 1257 Fg<sup>-1</sup> at 5 Ag<sup>-1</sup>, remained stable even at 125 Ag<sup>-1</sup>, with a Coulombic efficiency of nearly 100% and negligible capacitance degradation after 20,000 cycles, demonstrating effective energy storage capability via both diffusion and Faradaic mechanisms.

The MnCo<sub>2</sub>S<sub>4</sub>-NS material has a nanosheet structure tightly bonded to the graphite substrate without the use of a binder. The direct contact between the active material and the conductive substrate helped increase electron transport capability while enhancing the mechanical stability of the electrode. The MnCo<sub>2</sub>S<sub>4</sub>-NS electrode yielded a specific capacitance exceeding 2000 Fg<sup>-1</sup> at 2 Ag<sup>-1</sup>, maintaining over 90% capacity after 10,000 cycles.

The MnCo<sub>2</sub>S<sub>4</sub>/rGO composite material has a nanostructure combining MnCo<sub>2</sub>S<sub>4</sub> nanoparticles and rGO sheets, exhibiting superior electrochemical activity. This synergistic interaction enhanced the energy storage efficiency of the composite material compared to the two single components. The MnCo<sub>2</sub>S<sub>4</sub>/rGO electrode achieved a maximum specific capacitance of 3812.5 Fg<sup>-1</sup> at 2 Ag<sup>-1</sup>, still maintaining 1780.8 Fg<sup>-1</sup> at 50 Ag<sup>-1</sup>, and only dropped 7.8% in capacitance after 22,000 cycles.

Supercapacitor prototypes: Two symmetric supercapacitors,  $MnCo_2S_4-NS$  and  $MnCo_2S_4/rGO$ , were successfully fabricated. Among them, the sample using  $MnCo_2S_4/rGO$  yielded a specific capacitance of 316.2 Fg<sup>-1</sup> at 1 Ag<sup>-1</sup>, an energy density of 43.91 Whkg<sup>-1</sup>, and a power density of 505 Wkg<sup>-1</sup>, showing high application potential in high-energy and high-power supercapacitors.

#### RECOMMENDATIONS

- Continue to investigate more complex multi-metallic transition metal sulfides, especially combinations involving three or more elements, to exploit the synergistic effects between the redox centers.
- Integrating sulfide materials with other advanced carbon materials such as CNTs, graphene, or rGO can help form more robust hybrid electrode architectures with higher energy storage efficiency and longer cycle life.

#### NEW CONTRIBUTION OF THE THESIS

- Successful synthesis and detailed investigation of the structural, morphological, and electrochemical characteristics of CoS,  $CuCo_2S_4/rGO$ ,  $MnCo_2S_4-NS$  and  $MnCo_2S_4/rGO$  materials.
- Application of 3D printing technology in the fabrication of supercapacitor electrodes.
- Successful fabrication of two symmetric supercapacitor prototypes

- Proposing and analyzing the formation mechanism of transition metal sulfide materials, simultaneously clarifying the contribution of the two energy storage mechanisms – ion diffusion and surface Faradaic electrochemical reactions – during the charge-discharge process. The study also indicates the synergistic effect between the metal sulfide phase and the rGO network, which helps improve electrical conductivity, increase the density of active sites, and limit material aggregation, thereby optimizing the electrochemical performance of the electrode.

## DANH MỤC CÁC CÔNG TRÌNH ĐÃ CÔNG BỐ CỦA LUẬN ÁN

- 1. Ha M Nguyet, Le TT Tam, Doan T Tung, Nguyen T Yen, Hoang T Dung, Ngo T Dung, Le A Tuan, Phan N Minh, Le T Lu, "Facile synthesis of MnCo<sub>2</sub>S<sub>4</sub> nanosheets as a binder-free electrode material for high performance supercapacitor applications", New Journal of Chemistry, 46, 29, 13996-14003, 2022, (SCIE, Q1, IF = 3.3).
- 2. Le Thi Thanh Tam, Doan Thanh Tung, **Ha Minh Nguyet**, Nguyen Thi Ngoc Linh, Ngo Thanh Dung, Nguyen Van Quynh, Nguyen Van Dang, Dimitra Vernardou, Top Khac Le, Le Anh Tuan, Phan Ngoc Minh, Le Trong Lu, "High electrochemical performance of ink solution based on manganese cobalt sulfide/reduced graphene oxide nano-composites for supercapacitor electrode materials", RSC Advances, 12, 31, 20182-20190, 2022, (**SCIE**, **Q1**, **IF** = **3.9**)
- 3. Doan Thanh Tung, Le Thi Thanh Tam, Hoang Tran Dung, Ngo Thanh Dung, Phan Ngoc Hong, **Ha Minh Nguyet**, Nguyen Van-Quynh, Nguyen Van Chuc, Vu Quoc Trung, Le Trong Lu, Phan Ngoc Minh, "*Freeze gelation 3D printing of rGO-CuCo<sub>2</sub>S<sub>4</sub> nanocomposite for high-performance supercapacitor electrodes*", Electrochimica Acta, 138992, **2021**, (**SCIE**, **Q1**, **IF** = **7.3**).